Supplemental Document

# Compact intense extreme-ultraviolet source: supplement

**B. Major,[1,2,5,†] O. Ghafur,[3,†] K. Kovács,[4] K. Varjú,[1,2] V. Tosa,[4] M. J. J. Vrakking,[3] and B. Schütte[3,6]**

[1] *ELI-ALPS, ELI-HU Non-Profit Ltd., Wolfgang Sandner utca 3., Szeged 6728, Hungary*
[2] *Department of Optics and Quantum Electronics, University of Szeged, Dóm tér 9, Szeged 6720, Hungary*
[3] *Max-Born-Institut, Max-Born-Strasse 2A, 12489 Berlin, Germany*
[4] *National Institute for Research and Development of Isotopic and Molecular Technologies, Donat str. 67-103, 400293 Cluj-Napoca, Romania*
[5] *e-mail: Balazs.Major@eli-alps.hu*
[6] *e-mail: Bernd.Schuette@mbi-berlin.de*
[†] *These authors contributed equally to this paper.*



Supplement DOI: https://doi.org/10.6084/m9.figshare.14710020

Parent Article DOI: https://doi.org/10.1364/OPTICA.421564

## 1. EXPERIMENTAL METHODS

The experiments were performed using a Ti:sapphire laser system [1] operating at a central wavelength of 800 nm and delivering pulses with an energy up to 35 mJ and a duration of 40 fs. A pulse energy of up to 16 mJ was used in the current experiments. These pulses were focused using a spherical lens with a focal length of 1 m and coupled into the vacuum using a 3 mm thick fused silica window. The NIR beam waist radius in the focus was 50 µm. A pulsed gas jet was generated by a piezoelectric valve with a nozzle diameter of 1 mm that was mounted from above, applying a backing pressure of up to 10 bar. The laser crossed the gas jet very close to the exit of the nozzle, resulting in an effective interaction length of about 1.5 mm. The jet was operated at 10 Hz and had a duration of about 200 µs, leading to a background pressure in the vacuum chamber of $10^{-4}$ mbar. The relative position of the laser focus with respect to the gas jet was varied by mounting the lens on a long translation stage. A charge-coupled device (CCD) camera was used to record NIR beam profiles at the gas jet position.

A freestanding Al filter with a diameter of 15 mm and a thickness of 100 nm (Lebow) was used to block the fundamental laser. The XUV pulses were spectrally resolved using a diffraction grating, and the spectra were recorded using a microchannel plate (MCP) / phosphor screen assembly in combination with a CCD camera. The XUV beam profile was measured via the same detection method and using the grating in zeroth order. The XUV pulse energy was measured by an XUV photodiode (AXUV100G) that was temporarily placed at a distance of about 0.5 m behind the gas jet.

To generate high XUV intensities, the XUV pulses were refocused using a $B_4C$-coated spherical mirror with a focal length of 75 mm that was placed at a distance of 103 cm behind the gas jet. The focused XUV beam was intersected by a pulsed gas jet that was generated by a piezoelectric valve [2]. A molecular beam skimmer with an orifice diameter of 0.5 mm was used to select the central part of the atomic beam and to provide efficient differential pumping between the gas jet chamber and the interaction chamber. Photoions were generated in the interaction zone of a velocity-map imaging spectrometer [3], which was operated in spatial imaging mode [4]. The MCP / phosphor screen detector of the VMIS was gated to be able to separately record the ions in different charge states.

To determine the XUV Rayleigh length from the $Ar^{2+}$ ion distribution, the measurement shown in Fig. 5(a) was repeated at a lower gas density to avoid any possible space charge effects. The $Ar^{2+}$ ion yield scales with $I^2(z) \times w^2(z) \propto 1/w^4(z) \times w^2(z) = 1/w^2(z)$, assuming that two XUV photons are required for the generation of $Ar^{2+}$. Here $I(z)$ is the intensity as a function of the distance from the focal plane and $w(z) = w_0\sqrt{(1+z^2/z_R^2)}$ is the beam radius as a function of the distance from the focal plane. It follows that the $Ar^{2+}$ ion distribution is proportional to $(1+z^2/z_R^2)^{-1}$. This formula was used to fit the measured $Ar^{2+}$ ion distribution. In addition, the transverse $Ar^{2+}$ ion distribution was used to determine the spatial resolution after applying a Gaussian fit. Deconvolution of these two curves results in the extracted $Ar^{2+}$ ion distribution shown as a red curve in Fig. 5(c), from which a Rayleigh length of 6.5 $\mu$m was obtained. For comparison, we also show the convolution of the red and black curves as green dotted curve, which agrees well with the measured $Ar^{2+}$ distribution (blue curve).

## 2. NUMERICAL METHODS

### A. Non-adiabatic three-dimensional model of high-harmonic generation (HHG)

The HHG simulations were performed with an extended version of a three-dimensional nonadiabatic simulation code described in Ref. [5]. The model solves the paraxial wave equation in combination with the Lewenstein integral [6] to obtain the macroscopic response of a gas medium to a strong laser field. As a first step, propagation of the laser pulse ($E_l(z,r,t)$, with central angular frequency $\omega_l$) in the ionized medium is calculated assuming a cylindrical symmetry and taking into account the time- and space-dependent neutral dispersion (described by the refractive index $\eta_0$) and plasma dispersion (through the plasma angular frequency $\omega_p$), along with the optical Kerr effect (accounted for by the nonlinear refractive index $\bar{\eta}_2$)

$$\nabla^2 E_l(z,r,t) - \frac{1}{c^2}\frac{\partial^2 E_l(z,r,t)}{\partial t^2} = \frac{\omega_l^2}{c^2}\left(1-\eta_{\text{eff}}^2(z,r,t)\right)E_l(z,r,t)\,, \tag{S1}$$

where $c$ is the speed of light in vacuum, and the effective refractive index is

$$\eta_{\mathrm{eff}}(z,r,t) = \eta_0(z,r,t) + \bar{\eta}_2 \langle E_l^2(z,r,t)\rangle - \frac{\omega_p^2(z,r,t)}{2\omega_l^2}\,, \tag{S2}$$

$\langle E_l(t)\rangle$ meaning the optical-cycle average of the time-dependent electric field $E_l(t)$.

The dipole response of a single atom in the interaction volume is obtained using the strong-field approximation [6], given by

$$\begin{aligned} d_{\mathrm{nl}}(t) = 2\mathrm{Re}\Bigg\{ i\int_0^t \mathrm{d}t' \left[\frac{\pi}{\epsilon + i(t-t')/2}\right]^{3/2} E_l(t') \\ \times \Theta^*(p_{\mathrm{st}} - A_l(t)) \exp\left[-iS(p_{\mathrm{st}},t,t')\right] \Theta\big(p_{\mathrm{st}} - A_l(t')\big) + \mathrm{c.c}\Bigg\}\,. \end{aligned} \tag{S3}$$

In the previous expression, $p_{\mathrm{st}} = (1/(t-t'))\int_{t'}^t A_l(t'')\,\mathrm{d}t''$ is the stationary canonical momentum, and $S(p,t,t') = \int_{t'}^t \left[(p - A_l(t''))^2/2 + I_p\right]\mathrm{d}t''$ is the quasi-classical action. As is known, these quantities are defined by the vector potential of the laser field $A_l(t)$ and the ionization potential $I_p$ of the medium ($\epsilon$ being only a regularization constant). The dipole matrix element $\Theta$ used in the simulation are for a hydrogen-like potential [6]. The macroscopic response of the medium in a certain spatial grid point $(z,r)$ — taking into account the ionization rate $w(t)$ (based on the Ammosov-Delone-Krainov model) and the density of atoms $n_a$ — is

$$P_{\mathrm{nl}}(t) = n_a d_{\mathrm{nl}}(t) \exp\left[-\int_{-\infty}^t w(t')\,\mathrm{d}t'\right]\,. \tag{S4}$$

These macroscopic responses serve as source terms in each spatial grid point of the interaction medium when solving the wave equation of similar form as for the fundamental laser field (Eq. S1). During calculating the propagation of the harmonic field ($E_h(z,r,t)$) in the medium, neutral dispersion and absorption are taken into account:

$$\nabla^2 E_h(z,r,t) - \frac{1}{c^2}\frac{\partial^2 E_h(z,r,t)}{\partial t^2} = \mu_0 \frac{\mathrm{d}^2 P_{\mathrm{nl}}(z,r,t)}{\mathrm{d}t^2}\,, \tag{S5}$$

$\mu_0$ being the vacuum permeability. Eqs. S1 and S5 are solved in the Fourier domain. Propagation in vacuum on a distance of $\Delta z = z_2 - z_1$ between two planes (from $z_1$ to $z_2$) — like focusing of the laser field, free propagation after generation or backpropagation of the generated high-harmonic radiation — is carried out using the ABCD-Hankel transform [7]:

$$E(z_2,r,\omega) = -\frac{\mathrm{i}\omega}{cB}\exp\left(\mathrm{i}\frac{\omega D r^2}{2cB}\right)\exp\left(\mathrm{i}\frac{\omega}{c}\Delta z\right)\int_0^\infty E(z_1,\rho,\omega) J_0\left(\frac{\omega r\rho}{cB}\right)\exp\left(\mathrm{i}\frac{\omega A\rho^2}{2cB}\right)\rho\,\mathrm{d}\rho\,, \tag{S6}$$

where $J_0$ is the zeroth-order Bessel function of the first kind and the elements of the ABCD matrix describing the propagation between the two planes are also included.

### B. Simulation parameters

The simulation parameters are chosen to match the experimental conditions. The laser pulse with 800 nm central wavelength reaching the focusing element with $f = 1$ m focal length is assumed to have a Gaussian temporal envelope with a 40 fs intensity FWHM duration. The input laser beam has a $w = 8.5$ mm $1/e^2$-intensity radius and 11 mJ pulse energy. This way the beam size and the peak intensity at the jet ($z = 2.5$ cm behind the focus) matched the experimental values (200 µm and $4 \cdot 10^{14}$ W/cm$^2$, respectively). The slightly lower pulse energy in the simulation compared to the experimental value can be explained by the minor imperfections of the experimental beam, carrying some energy in low-intensity side lobes not contributing to HHG. The target medium — consisting of Kr atoms — is assumed to have a close-to-parabolic pressure profile along the main propagation axis $z$, matching the measured gas density profile (see Fig. S1). Along the perpendicular axis $r$ a homogeneous distribution is taken. The peak pressure of the medium was varied, with typical values around 800 mbar, corresponding to around 3 bar of backing pressure based on XUV refractive optics experiments and calculations [8]. Further geometrical conditions for the detection (XUV beam profile measurements, XUV focusing) are also matching experimental values, as described in the main text. In the propagation calculations after generation, the transmission of the Al filter and the reflectivity of the XUV focusing mirror are taken into account [9].

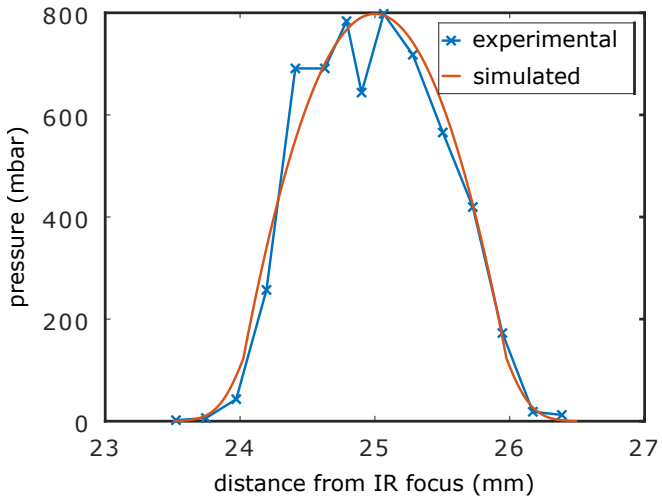


**Fig. S1.** The measured and simulated pressure profiles of the generation Kr medium along the propagation direction of the laser beam.

### C. Saturation of XUV yield with increasing pressure

The saturation of the HHG yield at >1 bar backing pressures — observed both in the experiments (see Fig. 1(a) of the manuscript) and in the simulations — is attributed to the reshaping of the laser field (see Fig. 3(a) of the manuscript). For a short explanation, we refer to the phase mismatch expression [10]:

$$\Delta k = \Delta k_g + \Delta k_d + \Delta k_n + \Delta k_p \,. \tag{S7}$$

Since the intensity of the beam is constant ($\mathrm{d}I/\mathrm{dz} = 0$) in the self-regulated volume, the dipole phase term in the phase mismatch is zero ($\Delta k_d = 0$). Also, the geometrical factor from the Gouy phase can be neglected ($\Delta k_g = 0$), since in this case the medium length is smaller than the Rayleigh length, and because of the ionization-induced guiding (similarly to phase matching in a guided geometry, see e.g. [11]). The remaining factors are the neutral and plasma dispersion terms, $\Delta k_n$ and $\Delta k_p$, respectively. The phase mismatch due to these components is proportional to the medium pressure $p$ ($\Delta k_n \sim p$ and $\Delta k_p \sim p$, see [10]), and hence the coherence length is inversely proportional to the density of the medium [10, 12]. Given that the absorption length is also inversely proportional to the density of the medium, it follows, according to the well-known formula of Constant *et al.* [12], that the high-harmonic yield is independent of pressure.

## REFERENCES


1. G. Gademann, F. Ple, P.-M. Paul, and M. J. J. Vrakking, "Carrier-envelope phase stabilization of a terawatt level chirped pulse amplifier for generation of intense isolated attosecond pulses," Opt. Express **19**, 24922 (2011).
2. D. Irimia, D. Dobrikov, R. Kortekaas, H. Voet, D. A. van den Ende, W. A. Groen, and M. H. M. Janssen, "A short pulse (7 µs fwhm) and high repetition rate (dc-5khz) cantilever piezovalve for pulsed atomic and molecular beams," Rev. Sci. Instrum. **80**, 113303 (2009).
3. A. T. J. B. Eppink and D. H. Parker, "Velocity map imaging of ions and electrons using electrostatic lenses: Application in photoelectron and photofragment ion imaging of molecular oxygen," Rev. Sci. Instrum. **68**, 3477 (1997).
4. M. Stei, J. von Vangerow, R. Otto, A. H. Kelkar, E. Carrascosa, T. Best, and R. Wester, "High resolution spatial map imaging of a gaseous target," J. Chem. Phys. **138**, 214201 (2013).
5. V. Tosa, E. Takahashi, Y. Nabekawa, and K. Midorikawa, "Generation of high-order harmonics in a self-guided beam," Phys. Rev. A **67**, 063817 (2003).
6. M. Lewenstein, P. Balcou, M. Y. Ivanov, A. L'Huillier, and P. B. Corkum, "Theory of high-harmonic generation by low-frequency laser fields," Phys. Rev. A **49**, 2117–2132 (1994).
7. B. Major, Z. L. Horváth, and K. Varjú, "Spatial characterization of light beams analyzed by cylindrical-grating slit-less spectrometers," Appl. Opt. **57**, 738–745 (2018).
8. L. Drescher, O. Kornilov, T. Witting, G. Reitsma, N. Monserud, A. Rouzée, J. Mikosch, M. J. Vrakking, and B. Schütte, "Extreme-ultraviolet refractive optics," Nature **564**, 91–94 (2018).

9. B. Major, M. Kretschmar, O. Ghafur, A. Hoffmann, K. Kovács, K. Varjú, B. Senfftleben, J. Tümmler, I. Will, T. Nagy, D. Rupp, M. J. J. Vrakking, V. Tosa, and B. Schütte, "Propagation-assisted generation of intense few-femtosecond high-harmonic pulses," J. Physics: Photonics **2**, 034002 (2020).
10. C. M. Heyl, H. Coudert-Alteirac, M. Miranda, M. Louisy, K. Kovacs, V. Tosa, E. Balogh, K. Varjú, A. L'Huillier, A. Couairon, and C. L. Arnold, "Scale-invariant nonlinear optics in gases," Optica **3**, 75–81 (2016).
11. T. Popmintchev, M.-C. Chen, O. Cohen, M. E. Grisham, J. J. Rocca, M. M. Murnane, and H. C. Kapteyn, "Extended phase matching of high harmonics driven by mid-infrared light," Opt. Lett. **33**, 2128–2130 (2008).
12. E. Constant, D. Garzella, P. Breger, E. Mével, C. Dorrer, C. Le Blanc, F. Salin, and P. Agostini, "Optimizing high harmonic generation in absorbing gases: Model and experiment," Phys. Rev. Lett. **82**, 1668–1671 (1999).